Combinatorial pulsed laser deposition of doped YIG films on YAG

A. Sposito[1,*], S.A. Gregory[1], P.A.J. de Groot[2], R.W. Eason[1]

[1] *Optoelectronics Research Centre, University of Southampton, SO17 1BJ, Southampton, United Kingdom*

[2] *Physics and Astronomy, University of Southampton, SO17 1BJ, Southampton, United Kingdom*

We investigate the crystalline growth of yttrium iron garnet (YIG) films doped with bismuth (Bi) and cerium (Ce) by combinatorial pulsed laser deposition (PLD), co-ablating a YIG target and either a Bi_2O_3 or a CeO_2 target, for applications in microwave and optical communications. Substrate temperature is critical for crystalline growth of YIG with simultaneous inclusion of Bi in the garnet lattice, whereas Ce is not incorporated in the garnet structure, but forms a separate CeO_2 phase.

* E-mail: as11g10@orc.soton.ac.uk.

I. INTRODUCTION

Magneto-optic garnets, such as yttrium iron garnet (YIG – $Y_3Fe_5O_{12}$), find applications in microwave devices (e.g. circulators and magneto-static wave filters)[1,2] and optical communications (e.g. Faraday rotators and isolators)[3,4]. In the latter field the Faraday rotation can be increased by substituting yttrium (Y) atoms in the YIG lattice with bismuth (Bi)[5] or cerium (Ce)[6]: in particular, it has been demonstrated that the Verdet constant increases linearly with doping concentration[6].

Unlike liquid phase epitaxy[7], where film growth happens in thermodynamic equilibrium, Pulsed Laser Deposition (PLD)[8] allows the growth of thermodynamically unstable materials, such as Bi:YIG and Ce:YIG even up to fully substituted garnets, such as BIG, ($Bi_3Fe_5O_{12}$), as already demonstrated in [9]. Moreover PLD has already proven to be a reliable film growth method for growing high-quality materials for lasing devices[10] and is a relatively inexpensive, fast and versatile deposition technique, whose set-up can be adjusted so that different targets can be ablated with different lasers either synchronously or sequentially, in order to tune material composition[11,12] or grow multi-layer structures[13,14] respectively.

We already optimized the growth of YIG on YAG (100)-oriented substrates by single-beam, single-target PLD in [15], where we observed a Fe-deficiency in all samples. Further experiments were conducted in our multi-beam, multi-target PLD (multi-PLD) system in order to observe the change of YIG film properties with composition[11].

In this paper we discuss our results on growth of doped YIG films by multi-PLD, by co-ablating a YIG target and either a Bi_2O_3 target or a CeO_2 target. In particular we show how the substrate temperature affects the doping level and the crystalline growth of Bi:YIG films; our multi-PLD attempts of growing Ce:YIG showed also that Ce is not incorporated as Ce^{3+} in the garnet lattice, but forms a separate crystalline CeO_2 phase intermixed with the YIG

phase, thus disrupting magnetic properties, such as domain wall nucleation and motion, of the iron garnet.

II. EXPERIMENTAL TECHNIQUES

All YIG films were grown on 10 × 10 mm^2 × 1 mm-thick YAG (100) substrates in our combinatorial (multi-PLD) system, described in detail in [16]. A frequency-quadrupled Nd:YAG laser, Continuum Surelite II-10 operating at $\lambda = 266$ nm (~5 ns pulse duration) with a fixed pulse repetition rate of 10 Hz, was used to ablate a polycrystalline YIG target (99.99% purity, Testbourne Ltd.); the Bi_2O_3 and the CeO_2 targets (99.99% purity, Testbourne Ltd.) were ablated by a Coherent CompexPro 102F KrF excimer laser operating at $\lambda = 248$ nm (20 ns pulse duration), whose repetition frequency f_{KrF} can be changed from 1 Hz to 20 Hz. A Synrad J48-2W carbon dioxide (CO_2) laser operating at 10.6 μm (max. output power: 40 W) was used to heat the substrate during the deposition. The distance between target and substrate was fixed at $d \approx 4$ cm. The Nd:YAG laser fluence was set at $F_{Nd:YAG} \approx (1.1 - 1.2)$ J/cm^2. The excimer laser fluence was set at $F_{KrF} \approx 2.1$ J/cm^2 for Bi:YIG experiments and $F_{KrF} \approx 1.0$ J/cm^2 for Ce:YIG depositions. The vacuum chamber was pumped down to a base pressure below 0.01 Pa and then filled with flowing oxygen gas at a pressure of $P_{O2} \approx 3.4$ Pa. The other growth conditions, i.e. substrate temperature (T) and KrF laser repetition rate, were changed to allow a parametric evaluation of optimum growth of Bi:YIG; for Ce:YIG depositions substrate temperature was set at the maximum value allowed in our multi-PLD system ($T \approx 1150$ K). All films were grown in 2 hours (i.e. ~72,000 Nd:YAG laser pulses), unless otherwise stated.

Optical microscopy and SEM (Zeiss Evo 50) were used for surface analysis of our samples. Compositional analysis was performed by EDX (Oxford Instruments INCA PentaFETx3): the instrument was energy-calibrated with a cobalt stub before measurements

and the YIG target and a blank YAG substrate were used for reference; oxygen concentration was assumed constant at 12 formula units and accuracy on the concentration of other elements (Bi, Ce, Y and Fe) is estimated to be ~0.04 formula units. Crystallographic analysis was performed by XRD (Bruker D2 Phaser), providing a resolution of 0.01°. A description of the set-up used to measure ferromagnetic resonance (FMR) linewidth, used as a film quality indicator (accuracy is ~0.1 mT), can be found in [11] and [15].

III. RESULTS AND DISCUSSION

A. Bi:YIG

When growing films containing Bi, the melting points of metallic Bi ($T_{m,\,Bi} \approx 545$ K) and of its oxide ($T_{m,\,Bi2O3} \approx 1090$ K) must be taken into account; moreover the depression of melting point of nanoparticles and materials in thin-film form must be considered too. Heating the substrate at temperatures $T > T_{m,\,Bi2O3}$ will lead to re-evaporation of both Bi and Bi_2O_3 species impinging on the substrate.

Attempts at growing Bi_2O_3 tester samples on *c*-cut sapphire (α-Al_2O_3) resulted in no film growth at temperatures $T \geq 1000$ K: although optical microscopy and profilometry revealed the presence of particulates scattered across the substrate surface, no film was revealed by stylus profiler and XRD analysis. Room temperature (RT) deposition allowed the growth of Bi_2O_3 on sapphire at a high deposition rate (~0.21 nm/pulse), but with an amorphous phase, as revealed by XRD analysis (no diffraction peak between $2\theta = 20°$ and 80°) of a ~15 μm-thick film grown in 1 hour at 20 Hz.

Following these first trials, we tried depositing Bi:YIG on YAG (100) substrates over a wide range of substrate temperatures, from RT up to the maximum $T \approx 1150$ K, fixing the KrF laser repetition rate at 1 Hz for most depositions: the results are summarised in Table I,

where pure YIG samples Y1, Y4 and Y5, grown under the same conditions as BY1a, BY4 and BY5a respectively, are listed for reference. Samples BY1b and BY5b were grown under the same conditions as BY1a and BY5a, respectively, but with the KrF laser set at 2 Hz.

TABLE I. Deposition conditions, FMR linewidth (ΔH), composition [formula units], colour of Bi:YIG samples BY1-9 and of YIG samples Y1, Y4 and Y5, used as a reference.

SAMPLE	Estimated substrate temperature [K]	f_{KrF} [Hz]	ΔH [mT]	Bi conc.	Y conc.	Fe conc.	Sample colour
Y1	1150	0	4.7	0.00	3.37	4.63	Yellow
BY1a	1150	1	6.2	0.07	3.32	4.61	Yellow
BY1b	1150	2	6.2	0.13	3.27	4.60	Yellow
BY2	1050	1	7.9	0.07	3.36	4.57	Yellow
BY3	1000	1	10.0	0.06	3.27	4.66	Yellow
Y4	950	0	19.2	0	3.31	4.69	Yellow
BY4	950	1	13.2	0.22	3.20	4.57	Yellow
Y5	900	0	23.4	0	3.29	4.71	Dark yellow
BY5a	900	1	8.8	0.22	3.45	4.32	Yellow
BY5b	900	2	10.4	0.30	3.33	4.38	Yellow
BY6	875	1	12.2	0.30	3.28	4.42	Yellow
BY7	850	1	54.5	1.49	3.04	3.47	Dark yellow
BY8	750	1	–	2.94	2.14	2.91	Orange/red
BY9	300	1	–	3.16	1.96	2.88	Black/red

All Bi:YIG samples grown at temperature $T \geq 875$ K feature the yellow colour typical of Fe-deficient YIG films[15], whereas the reference YIG sample Y5 is dark yellow at $T \approx 900$ K. At $T \approx 850$ K the Bi:YIG film colour becomes darker and then orange with a red tint at $T \approx 750$ K. The sample grown at RT (~300 K), although showing good specular reflection, in transmission appears black with a faint red tint (effectively zero transmission). As already shown in [15], the film colour is an indicator of crystal quality. XRD analysis showed that Bi:YIG samples BY1-BY6 only have crystalline YIG (100) peaks, whereas the XRD pattern of BY7 (shown in Figure 1) features two distinct BIG and YIG peaks, respectively at $2\theta \approx 28.24°$ and $2\theta \approx 28.86°$. BY8 shows no evidence of any garnet phase, with only a peak at $2\theta \approx 29.2°$, that can be attributed to (111)-oriented Y_2O_3 (shown via the (222) peak, as in Figure 1); BY9 does not show any crystalline phase, as no diffraction peaks are observed in

its XRD pattern, except for those attributable to the YAG substrate. Table II shows the database peak positions for BIG (400), YIG (400), YAG (400) and Y_2O_3 (222) for reference.

TABLE II. Database peak positions for BIG, YIG and YAG (100) phases and Y_2O_3 (111) and relative references.

XRD peak:	**BIG (400)**	**YIG (400)**	**YAG (400)**	**Y_2O_3 (222)**
Database peak position:	28.22°	28.90°	29.80°	29.20°
Reference:	[17]	[18]	[19]	[20]

XRD analysis of samples BY1-BY6, grown at $T \geq 875$ K, showed a shift of the YIG peak position with changing substrate temperature, as shown in Figure 2: while the XRD patterns of pure YIG samples Y1, Y4 and Y5 feature a YIG (400) peak at roughly the same diffraction angle, the YIG (400) peak in Bi:YIG films tends to shift towards lower diffraction angles with decreasing substrate temperature, implying an increase in lattice constant.

Figure 3 shows the variation of film composition for Bi:YIG samples grown at $f_{KrF} = 1$ Hz with substrate temperature. As shown also in Table 1, the film composition changes dramatically with temperature and a transition region is clearly observed around $T \approx 850$ K, the same range of temperature where the change in crystallinity is observed, as discussed above.

Figure 4 shows the trend of FMR linewidth with substrate temperature: as already found in [15] for pure YIG films grown by PLD with a KrF laser, FMR linewidth tends to increase with decreasing temperature, but more slowly for Bi:YIG films, compared to pure YIG (Y1, Y4 and Y5); also, at a temperature $T \approx 900$ K there appears to be a local minimum for FMR linewidth, as opposed to the values for pure YIG, where the lowest value is at $T \approx 1150$ K and increases steadily with decreasing temperature.

The observed phenomena require further discussion to try to identify the primary cause of change of YIG properties with substrate temperature, Bi concentration and crystallinity. At very high temperatures ($T \geq 1000$ K) only a small fraction of the bismuth present within the

plume is incorporated into the final garnet structure, because of re-evaporation from the hot surface of the sample, resulting in a very low doping level (~0.07 formula units – see Table I), which causes a small change in lattice constant (see Figure 2), due to the larger ionic radius of Bi, compared to Y. This doping level is also too low to cause a significant change in magnetic properties and FMR linewidth ΔH initially increases with decreasing temperature (see Figure 4), as already observed in [15] for YIG films. At $T \approx$ (900 – 950) K the Bi doping increases by a factor of ~3 (~0.22 formula units – see Table I), suggesting that the substrate temperature is closer to the melting point of Bi_2O_3 in thin-film form, and the lattice constant increases accordingly (as seen in the large YIG (400) peak shift in Figure 2, ~0.17° between BY5a and BY1a); it is at $T \approx$ 900 K (BY5a) that the local minimum of $\Delta H(T)$ is observed and this can be explained with the change in YIG film properties with Bi doping. Also our results agree with previous findings in the literature of PLD growth of Bi:YIG by single-beam single-target PLD, where optimum growth temperatures of ~900 K for Bi:YIG on GGG [21,22] and ~1100 K for YIG on GGG [1,22,23] are reported.

Two factors can be taken into account to explain the change in the FMR linewidth trend with substrate temperature:

1) a direct change of magnetic properties of YIG with Bi doping;

2) an indirect effect of Bi doping on magnetic properties via a change in crystallinity.

Regarding the first aspect of Bi inclusion, Figure 5 shows the variation of FMR linewidth with Bi concentration: although there is an increase of FMR linewidth with Bi concentration, the trend is not systematic (e.g. the Bi doping of BY3 is one fifth that of BY5b, but they have roughly the same FMR linewidth); also, there is no significant change in FMR linewidth, when doubling the KrF laser repetition rate (f_{KrF}) and thus doubling the Bi concentration at $T \approx$ 1150 K (BY1a and BY1b – see Table 1 and Figures 4 and 5). Also, when doubling f_{KrF} at T

≈ 900 K (samples BY5a and BY5b), the Bi concentration increases by ~36%, but the FMR linewidth increases by ~18% (see Table 1 and Figures 4 and 5), meaning that Bi doping has a more dramatic role when it reaches a level higher than 0.2 formula units.

On the other hand, the second factor is reinforced by a clear change in lattice constant with changing temperature (see Figure 2) and by the decreasing trend of YIG (400) peak position (i.e. an increase in lattice constant) with increasing Bi concentration, shown in Figure 6, as expected from theory, due to the larger ionic radius of Bi compared to Y. While the change in YIG peak position and lattice constant is clearly due to Bi doping, no change in YIG peak position with temperature is observed in pure YIG films (see Figure 2); however, at very high temperature ($T \geq 1000$ K) the deterioration of crystal quality has a stronger effect than that of Bi doping (quite low, ~0.07 formula units), which prevails only at $T \approx 900$ K – BY5a, and the observed local minimum of $\Delta H(T)$. A further decrease in temperature causes further deterioration of crystal quality, until at $T \approx 850$ K the substrate temperature probably reaches the depressed melting point of Bi_2O_3 ($T_{m,\ Bi2O3}$) and Bi concentration increases abruptly at 1.49 formula units, whereas both Y and Fe concentration decrease (see BY7 in Table I and Figure 3): this is the most likely cause of the formation of two separate BIG and YIG phases in the film (BY7 in Figure 1), which are detrimental for magnetic properties (see point BY7 in Figure 4). A further decrease in substrate temperature ($T \approx 750$ K) leads to the growth of an yttria phase (see BY8 in Figure 1) heavily doped with Bi and Fe, at similar concentrations (~3 formula units – see BY8 in Figure 3). The completely different crystal phase produces no magnetic properties and no FMR absorption. Growth at RT results in an amorphous film (BY9) with composition similar to BY8 and again no FMR.

To sum up, there is a complex interplay between substrate temperature (T), Bi concentration (Bi conc.), YIG peak position (2θ), crystal quality and FMR linewidth (ΔH), whose general trends are summarised schematically in Figure 7.

Finally we tried to grow a highly doped Bi:YIG film using a substrate temperature $T \approx$ 900 K, considered as a compromise between Bi-doping level and crystalline and magnetic properties. Setting the KrF laser repetition rate at f_{KrF} = 10 Hz resulted in a heavily doped Bi:YIG film, with a composition of $Bi_{2.38}Y_{2.81}Fe_{2.81}O_{12}$, showing a strong Fe deficiency and a low Y-substitutional level, suggesting that Bi is probably substituting Fe rather than Y, as already observed in BY7-BY9. The film featured also an XRD pattern similar to that of BY7, with two separate YIG and BIG peaks, and an FMR linewidth $\Delta H \approx 47.8$ mT. This eventually suggests that Bi doping level plays a big role: if excessive and substituting for Fe instead of Y, it causes the formation of different crystalline phases, which results in a large broadening of FMR linewidth.

B. Ce:YIG

Cerium and its oxides have higher melting points than bismuth and its oxides: $T_{m,\ Ce} \approx$ 1068 K, $T_{m,\ Ce2O3} \approx$ 2450 K and $T_{m,\ CeO2} \approx$ 2673 K, which would therefore indicate that deposition of Ce:YIG films at high temperatures should be feasible. We tried co-ablating the CeO_2 target with the KrF laser set at $F_{KrF} \approx 1$ J/cm^2 and f_{KrF} = (1 – 2) Hz and the YIG target with the Nd:YAG laser set at $F_{Nd:YAG} \approx 1.1$ J/cm^2 and f_{KrF} = 10 Hz. The depositions were performed under the usual near-optimum growth conditions for YIG, i.e. at $T \approx 1150$ K, $P_{O2} \approx 3.3$ Pa and $d \approx 4$ cm.

Both samples grown at f_{KrF} = 1 and 2 Hz feature the typical yellow colour of YIG films, but two clearly distinct phases in the XRD patterns, as shown in Figure 8, and attributable to YIG (100) and CeO_2 (111). This suggests that the Ce^{4+} species ablated from the CeO_2 target are neither reduced nor included in the garnet lattice, but instead they form a separate phase intermixed with the YIG crystal structure, resulting in an absence of FMR absorption. The composition of the two films is: $Ce_{0.64}Y_{3.1}Fe_{4.26}O_{12}$ and $Ce_{1.61}Y_{2.67}Fe_{3.72}O_{12}$ for the samples

grown respectively at f_{KrF} = 1 Hz and f_{KrF} = 2 Hz, showing that, as in Bi:YIG films, not only the concentration of Y, but also that of Fe tends to decrease with increasing level of Ce doping.

No further multi-PLD experiments were performed for Ce inclusion because no FMR absorption was observed in our intended Ce:YIG samples; we instead investigated the ablation of the CeO_2 target and the growth of cerium oxide on *c*-cut sapphire substrates, heated at high temperature ($T \approx 1150$ K).

The CeO_2 target was ablated with the KrF laser, set at f_{KrF} = 20 Hz and different fluences ($F_{KrF} \approx 1$ and 2 J/cm^2), and with different background gases (oxygen, O_2, and argon, Ar). XRD analysis (see Figure 9) showed that the film grown in O_2 at $F_{KrF} \approx 2$ J/cm^2 is polycrystalline CeO_2 with two different orientations: (111) and (100). When depositing at lower fluence ($F_{KrF} \approx 1$ J/cm^2), either in O_2 or Ar, the film grows as CeO_2 (111). For all cases however, as confirmed also by EDX, the film composition was CeO_2, meaning that Ce species ablated from the CeO_2 target maintain the 4+ valence state, even in an Ar ambient, as reported in literature for a wide range of deposition conditions [24-28]. Growth rates were: ~0.069 nm/pulse and ~0.035 nm/pulse in O_2, respectively at $F_{KrF} \approx 2$ J/cm^2 and 1 J/cm^2, and ~0.028 nm/pulse in Ar at $F_{KrF} \approx 1$ J/cm^2.

The results of depositions of cerium oxide on sapphire substrates under different conditions confirmed what we had already observed in the attempts of growing Ce:YIG films: the cerium in the plume is incorporated in the film as crystalline CeO_2 with (111) preferential orientation.

V. CONCLUSIONS

We have investigated the possibility of growing doped YIG films by combinatorial PLD, in particular the growth of Bi:YIG and Ce:YIG by co-ablation of a YIG target with a frequency-quadrupled Nd:YAG laser and either a Bi_2O_3 or a CeO_2 target with a KrF laser.

The re-evaporation of Bi from the hot substrate surface limits the Bi-doping level at the high temperatures needed for optimum YIG growth, due to the lower melting points of Bi and its oxide. Lower substrate temperatures cause an increase in Bi concentration, but also degraded crystal quality and a resultant higher FMR linewidth. We found a compromise at a local minimum of FMR linewidth vs. substrate temperature ($T \approx 900$ K), before a critical deterioration of crystal quality and magnetic properties takes place; however, increasing the Bi-doping at this temperature will deteriorate both crystallinity and FMR, probably due to the fact that Bi is replacing not only Y, but also Fe atoms in the YIG lattice. This could be overcome by multi-PLD of Bi_2O_3, Y_2O_3 and Fe_2O_3 and ablating the 3 targets sequentially one at a time, in order to grow monolayers of each material and thus an artificial Bi:YIG crystal; however the film growth rate would be considerably lower.

Ce and its oxides have higher melting points than Bi and Bi_2O_3, thus allowing growth of heavily doped Ce:YIG at high temperatures. However, the lack of Ce_2O_3 targets and the fact that the ablated species from a CeO_2 target maintain their 4+ valence state do not allow the inclusion of Ce into the YIG lattice as Ce^{3+}, so that multi-PLD of YIG and CeO_2 produces polycrystalline films with intermixed CeO_2 and YIG phases and no FMR. The problem may be overcome using a metallic Ce target, although it tarnishes slowly in air, its ablation may cause formation of droplets and its ablated species may be easily oxidised in the wrong valence state in oxygen; however multi-PLD growth of Ce:YIG may be feasible in Ar.

The results presented in this paper show the potentials of multi-PLD to grow materials with engineered composition, for example in microwave and magneto-optic applications.

However, care must be taken in the choice of deposition conditions and targets, to ensure growth of the desired final material in the correct phase.

ACKNOWLEDGMENTS

The research was funded by the Engineering and Physical Sciences Research Council (EPSRC). Grants: EP/F019300/1, EP/G060363/1 and EP/J008052/1.

The authors would like to thank Dr. Kate Sloyan in the PLD research group of the Optoelectronics Research Centre of the University of Southampton for discussion and help with PLD, Dr. Mark E. Light in the University of Southampton School of Chemistry for his help with XRD analysis.

REFERENCES

[1] S. A. Manuilov, R. Fors, S. I. Khartsev, and A. M. Grishin, J. Appl. Phys. **105,** 033917 (2009).

[2] G. B. G. Stenning, G. J. Bowden, L. C. Maple, S. A. Gregory, A. Sposito, R. W. Eason, N. I. Zheludev, and P. A. J. De Groot, Opt. Express **21,** 1456 (2013).

[3] B. Lei, H. Juejun, J. Peng, K. Dong Hun, G. F. Dionne, L. C. Kimerling, and C. A. Ross, Nat. Photonics **5,** 758 (2011).

[4] H. Dotsch, N. Bahlmann, O. Zhuromskyy, M. Hammer, L. Wilkens, R. Gerhardt, P. Hertel, and A. F. Popkov, J. Opt. Soc. Am. B **22,** 240 (2005).

[5] H. Hayashi, S. Iwasa, N. J. Vas, T. Yoshitake, K. Ueda, S. Yokoyama, S. Higuchi, H. Takeshita, and M. Nakahara, Appl. Surf. Sci. **197,** 463 (2002).

[6] S. Higuchi, K. Ueda, F. Yahiro, Y. Nakata, H. Uetsuhara, T. Okada, and M. Maeda, IEEE Trans. Magn. **37,** 2451 (2001).

[7] H. X. Wei and W. S. Wang, IEEE Trans. Magn. **20,** 1222 (1984).

[8] R. W. Eason, ed.: *Pulsed Laser Deposition of Thin Films – Applications-led Growth of Functional Materials* (Wiley Interscience, 2007).

[9] S. Kahl and A. M. Grishin, J. Appl. Phys. **93,** 6945 (2003).

[10] N. A. Vainos, C. Grivas, C. Fotakis, R. W. Eason, A. A. Anderson, D. S. Gill, D. P. Shepherd, M. Jelinek, J. Lancok, and J. Sonsky, Appl. Surf. Sci. **127,** 514 (1998).

[11] A. Sposito, S. A. Gregory, G. B. G. Stenning, P. A. J. de Groot, and R. W. Eason, "Compositional tuning of YIG film properties by multi-beam pulsed laser deposition," IEEE Photon. J. (submitted, Nov. 2013).

[12] M. S. B. Darby, T. C. May-Smith, and R. W. Eason, Appl. Phys. A Mater. Sci. Process. **93,** 477 (2008).

[13] K. A. Sloyan, T. C. May-Smith, M. N. Zervas, and R. W. Eason, Appl. Phys. Lett. **101,** 081117 (2012).

[14] K. A. Sloyan, T. C. May-Smith, M. Zervas, R. W. Eason, S. Huband, D. Walker, and P. A. Thomas, Opt. Express **18,** 24679 (2010).

[15] A. Sposito, T. C. May-Smith, G. B. G. Stenning, P. A. J. de Groot, and R. W. Eason, Opt. Mater. Express **3,** 624 (2013).

[16] T. C. May-Smith, K. A. Sloyan, R. Gazia, and R. W. Eason, Cryst. Growth Des. **11,** 1098 (2011).

[17] H. Toraya and T. Okuda, J. Phys. Chem. Solids **56,** 1317 (1995).

[18] D. Rodic, M. Mitric, R. Tellgren, H. Rundloef, and A. Kremenovic, J. Magn. Magn. Mater. **191,** 137 (1999).

[19] L. Dobrzycki, E. Bulska, D. A. Pawlak, Z. Frukacz, and K. Wozniak, Inorg. Chem. **43,** 7656 (2004).

[20] G. Baldinozzi, J. F. Berar, and G. Calvarin, Mater. Sci. Forum **278-281,** 680 (1998).

[21] E. Popova, L. Magdenko, H. Niedoba, M. Deb, B. Dagens, B. Berini, M. Vanwolleghem, C. Vilar, F. Gendron, A. Fouchet, J. Scola, Y. Dumont, M. Guyot, and N. Keller, J. Appl. Phys. **112,** 093910 (2012).

[22] B. M. Simion, G. Thomas, R. Ramesh, V. G. Keramidas, and R. L. Pfeffer, Appl. Phys. Lett. **66,** 830 (1995).

[23] S. Yiyan, S. Young-Yeal, C. Houchen, M. Kabatek, M. Jantz, W. Schneider, W. Mingzhong, H. Schultheiss, and A. Hoffmann, Appl. Phys. Lett. **101,** 152405 (2012).

[24] S. Amirhaghi, Y. H. Li, J. A. Kilner, and I. W. Boyd, Mater. Sci. Eng. B **34,** 192 (1995).

[25] R. P. Wang, S. H. Pan, Y. L. Zhou, G. W. Zhou, N. N. Liu, K. Xie, and H. B. Lu, J. Cryst. Growth **200,** 505 (1999).

[26] D. Q. Shi, M. Ionescu, J. McKinnon, and S. X. Dou, Physica C **356,** 304 (2001).

[27] R. Bhattacharya, T. Chaudhuri, and S. Phok, Thin Solid Films **515,** 6971 (2007).

[28] Y. T. Ho, K. S. Chang, K. C. Liu, L. Z. Hsieh, and M. H. Liang, Cryst. Res. Technol. **48,** 308 (2013).

List of figures:

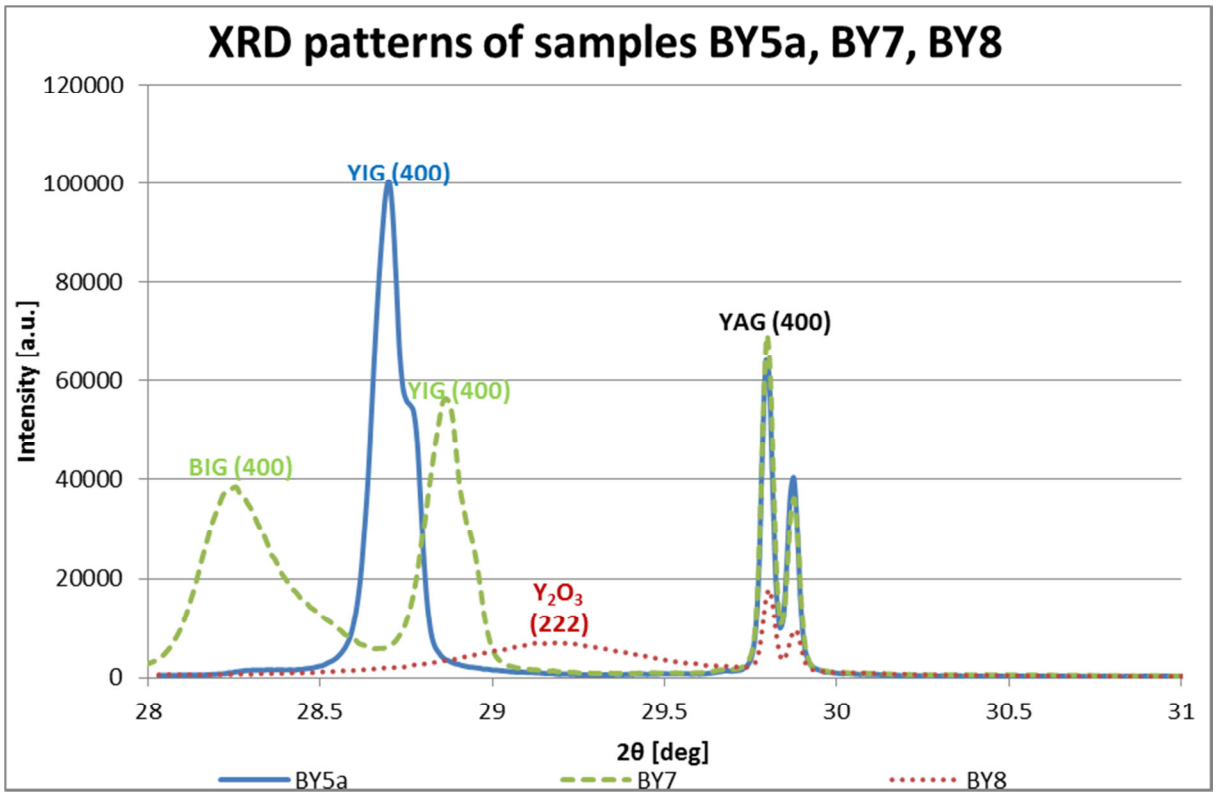

FIG. 1. Comparison of XRD patterns of BY5a, BY7 and BY8.
Peak doublets are due to Cu-$K_{\alpha 2}$ radiation present in the diffractometer.

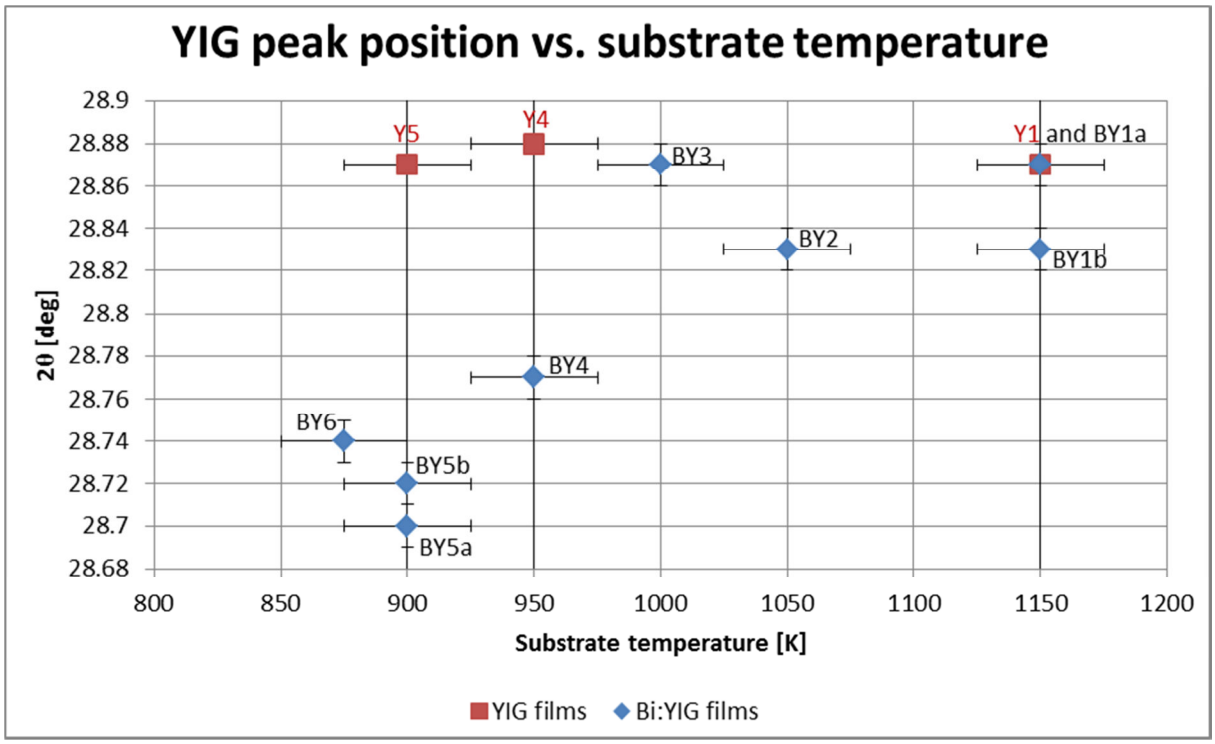

FIG. 2. Trend of YIG (400) peak position in the XRD patterns of YIG and Bi:YIG films with substrate temperature. Error bars are shown: $\Delta T = \pm 25$ K, $\Delta 2\theta = \pm 0.01°$.

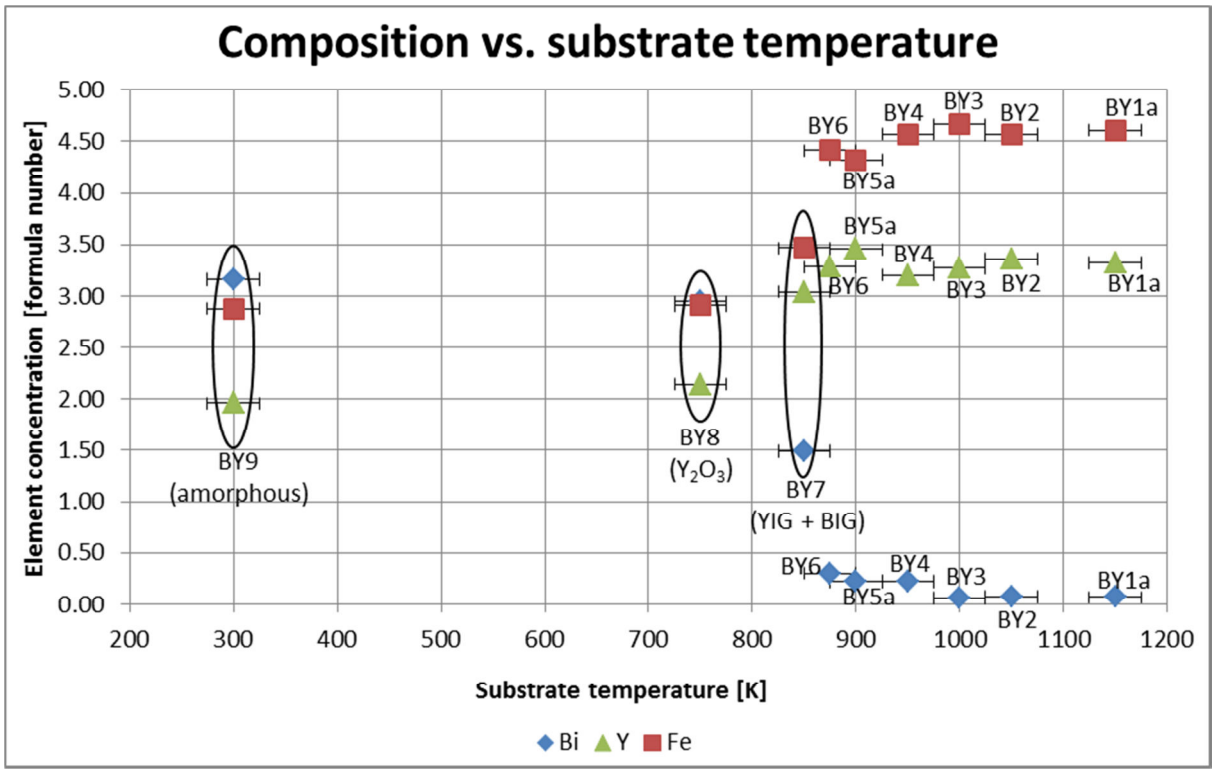

FIG. 3. Trend of composition with substrate temperature.
The samples highlighted with ellipses have peculiar crystallinity, as shown here and in Figure 1.
Error bars are shown for temperature (ΔT = ±25 K); the accuracy of compositional analysis is: ±0.04 formula numbers.

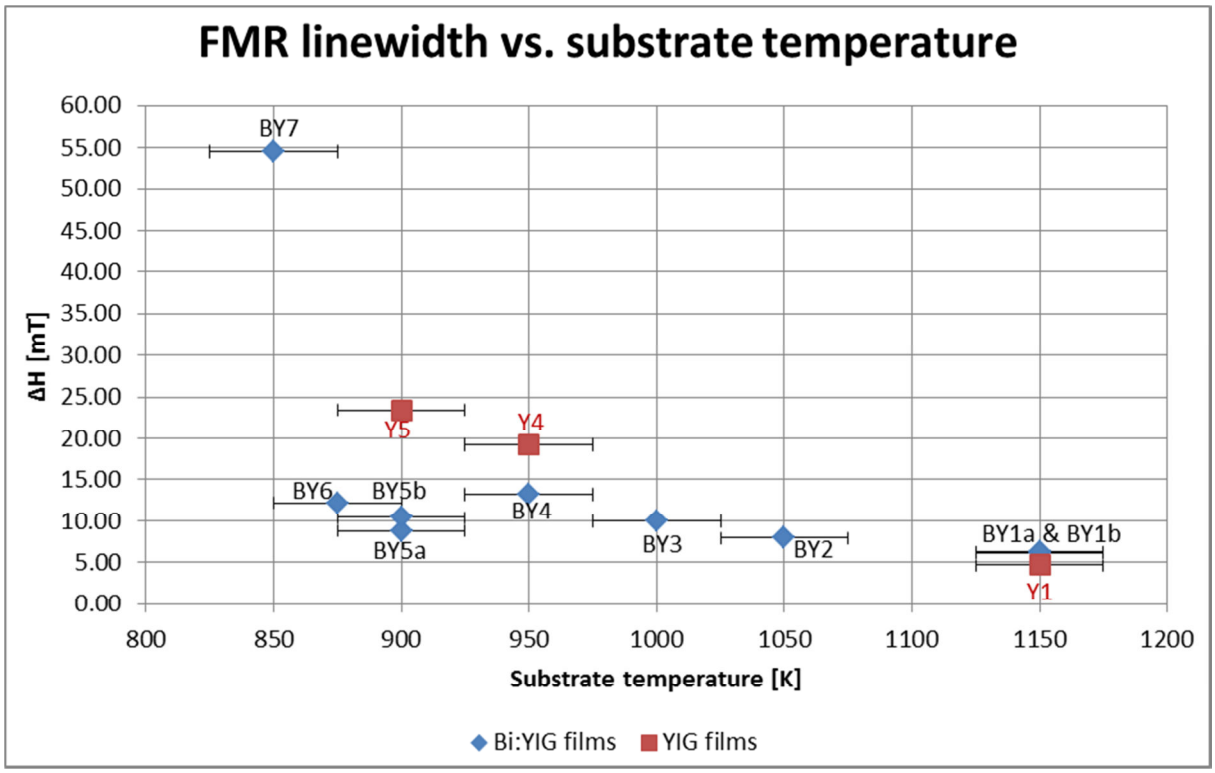

FIG. 4. Trend of FMR linewidth with substrate temperature.
Error bars are shown for temperature ($\Delta T = \pm 25$ K); the accuracy of FMR linewidth measurements is: ~0.1 mT.

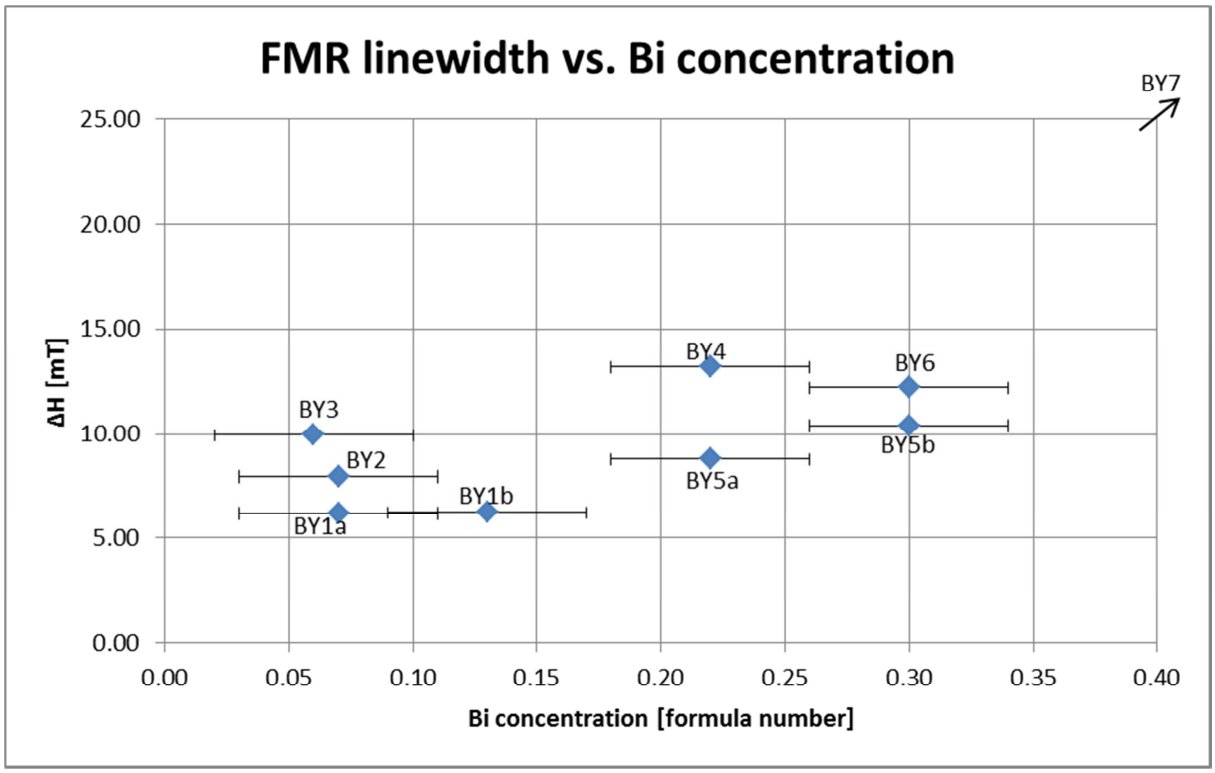

FIG. 5. Trend of FMR linewidth with Bi concentration.
Error bars are shown for Bi concentration (±0.04 formula numbers); the accuracy of FMR linewidth measurements is: ~0.1 mT.

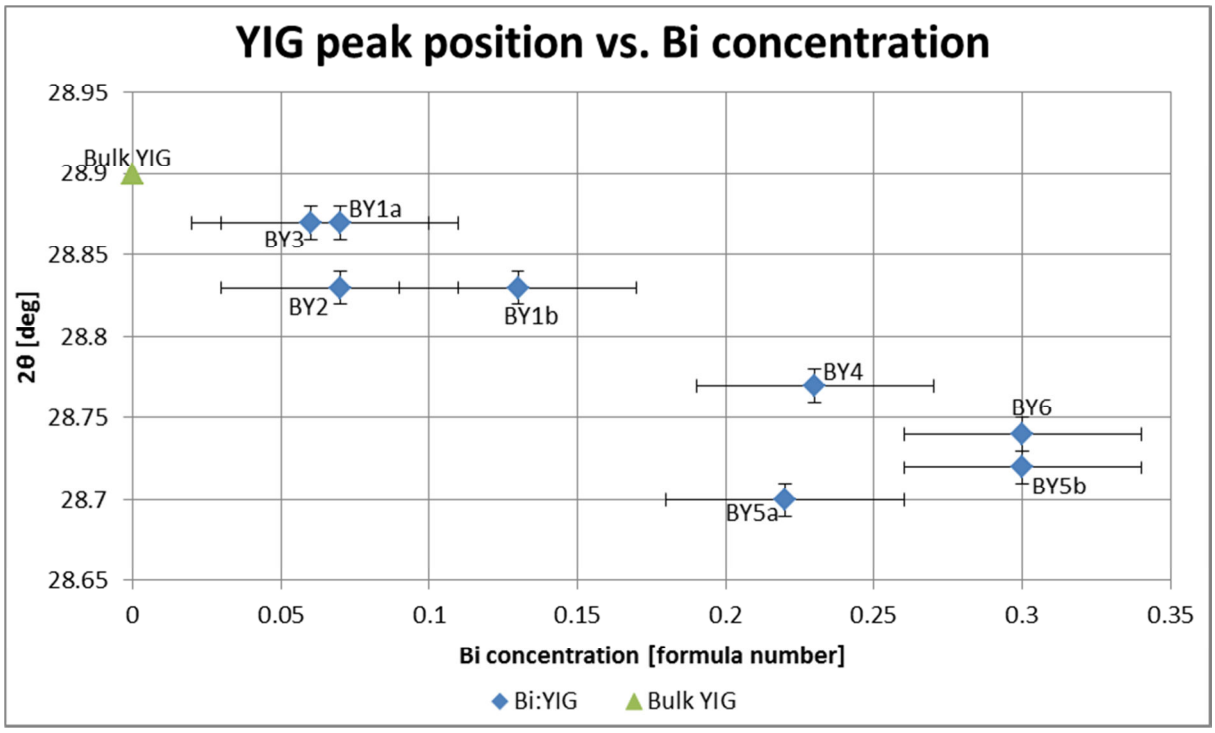

FIG. 6. Trend of YIG (400) peak position with Bi concentration.
Error bars are shown for Bi concentration (±0.04 formula numbers) and $\Delta 2\theta = \pm 0.01°$.

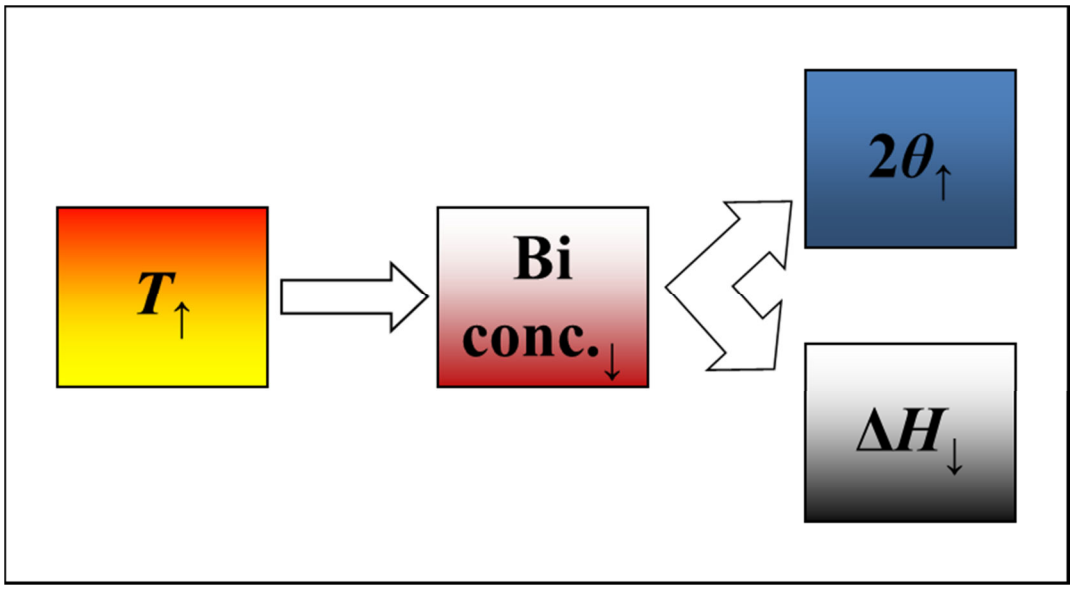

FIG. 7. Schematic of the interplay between substrate temperature (T), Bi concentration (Bi conc.), YIG peak position (2θ) and FMR linewidth (ΔH) in the multi-PLD growth of Bi:YIG.

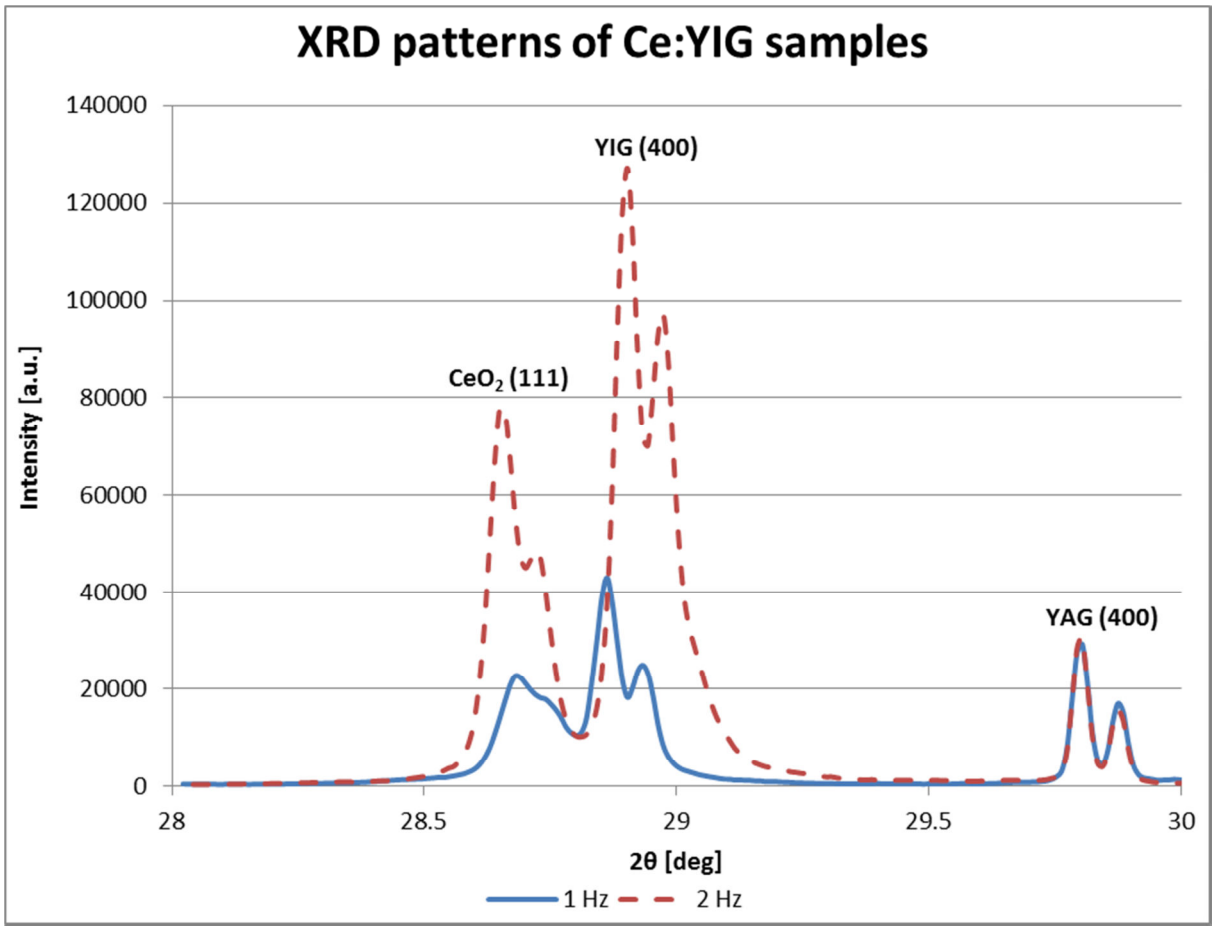

FIG. 8. XRD patterns of Ce:YIG samples.
Peak doublets are due to Cu-$K_{\alpha 2}$ radiation present in the diffractometer.

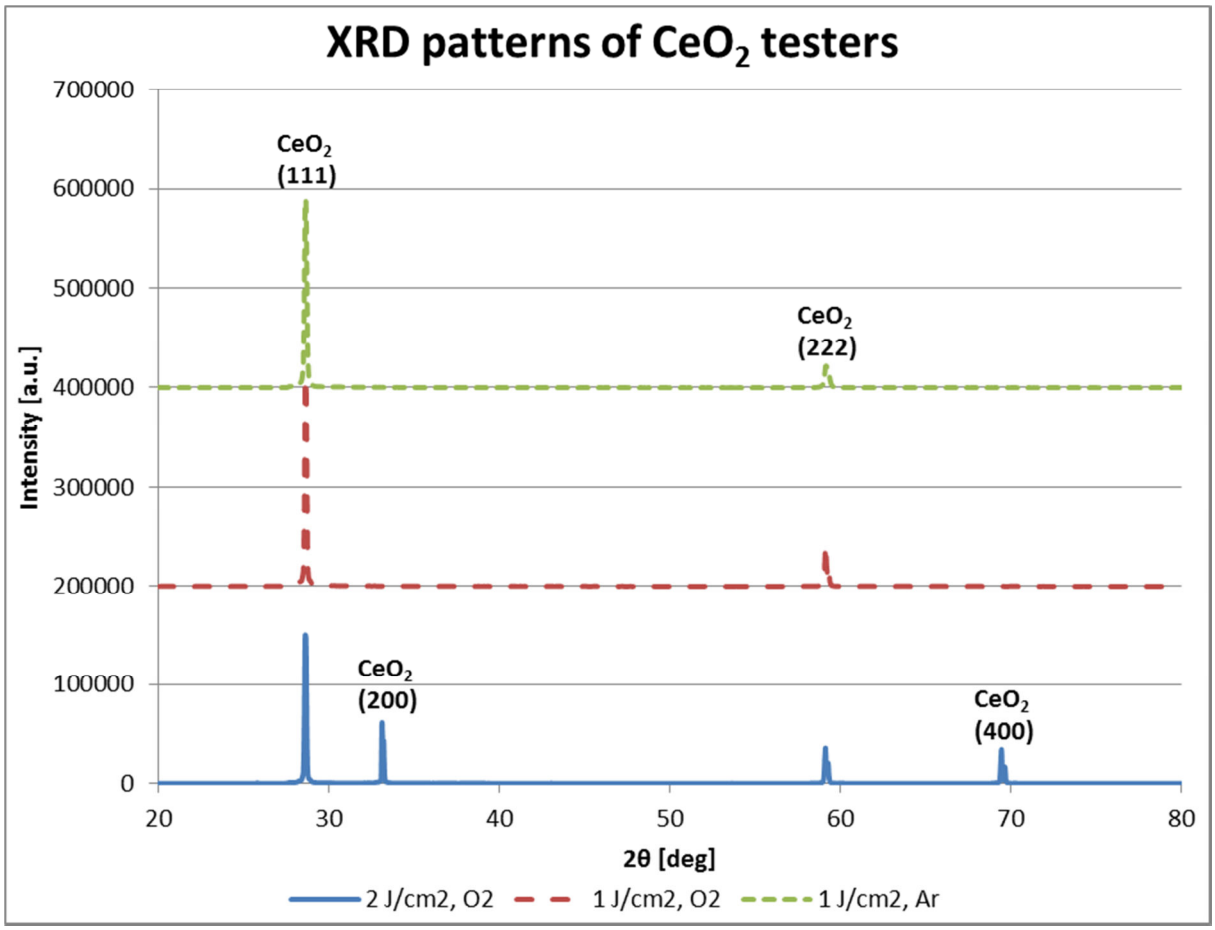

FIG. 9. Comparison of XRD patterns of CeO_2 test films.